

Probing the phonon dispersion relations of graphite from the double-resonance process of Stokes and anti-Stokes Raman scatterings in multiwalled carbon nanotubes

PingHeng Tan,^{1,2,*} Long An,² LuQi Liu,³ ZhiXin Guo,³ Richard Czerw,⁴ David L. Carroll,⁴ Pulickel M. Ajayan,⁵ Nai Zhang,⁶ and HongLi Guo⁶

¹Walter Schottky Institut, Technische Universität München, D-85748 Garching, Germany

²National Laboratory for Superlattices and Microstructures, P. O. Box 912, Beijing 100083, People's Republic of China

³Institute of Chemistry, Chinese Academy of Sciences, Beijing 110015, People's Republic of China

⁴Department of Physics and Astronomy, Clemson University, Clemson, South Carolina 29634

⁵Department of Materials Science and Engineering, Rensselaer Polytechnic Institute, Troy, New York

⁶Laboratory center, Research Institute of Petroleum Exploration and Development, P. O. Box 910, Beijing 100083, People's Republic of China

(Received 12 March 2002; revised manuscript received 8 July 2002; published 13 December 2002)

The Stokes and anti-Stokes Raman spectra of a multiwalled carbon nanotube (MWNT) sample are studied here by four excitation energies and the observed Raman modes are assigned based on the double resonance Raman effect and the previous results in graphite whiskers. There exists frequency discrepancy between Stokes and anti-Stokes lines (FDSA) of many Raman modes in MWNT's and the discrepancy values are strongly dependent on the excitation energy, in which the FDSA value of the D' mode even changes from a positive value (9 cm^{-1} , 1.58 eV) to a negative value (-11 cm^{-1} , 2.54 eV). The laser-energy dependence of the FDSA values of some modes in MWNT's is attributed to the nonlinear frequency dependence of Stokes and anti-Stokes Raman lines of these modes on the excitation energy. Raman results and the theoretical analysis of the intravalley and intervalley double resonance processes of Stokes and anti-Stokes Raman scatterings both show that the frequency of an anti-Stokes peak excited by ε_L is equal to that of the corresponding Stokes peak excited by a laser excitation of $\varepsilon_L + \hbar\omega_S$ where $\hbar\omega_S$ is the phonon energy of the Raman mode. Stokes and anti-Stokes double-resonance Raman scatterings have been used to probe the phonon dispersion relations of graphite. The Raman data of the well-known disorder-induced D mode are in good agreement with the theoretical results.

DOI: 10.1103/PhysRevB.66.245410

PACS number(s): 78.30.Na, 63.20.Kr, 81.05.Tp, 63.22.+m

I. INTRODUCTION

In the Raman spectra of disordered graphite, in addition to two in-plane Raman active E_{2g} modes located at ~ 42 and $\sim 1582\text{ cm}^{-1}$ (G band), there is an additional disorder-induced D band which appears at about 1350 cm^{-1} for green laser excitation.^{1,2} The D mode also appears in the Raman spectra of purified multiwalled carbon nanotube (MWNT)^{3,4} and single-walled carbon nanotube samples.^{6,5} In contrast to the Raman peaks in other crystals, the frequency of the well-known D band exhibits two important spectral features. First, the D -band frequency is highly dispersive and shifts with excitation energy at a rate of $44\text{--}53\text{ cm}^{-1}$ over a wide excitation energy (ε_L) range for different sp^2 carbon materials.^{6–18} Second, the Stokes (ω_S) and anti-Stokes (ω_{AS}) components of the D -band in graphite materials^{7,13,19} have different frequencies, and the frequency difference is equal to the product of the phonon energy ($\hbar\omega_S$) of the D mode and its laser-energy dispersion $\partial\omega_S/\partial\varepsilon_L$.⁷ There exists similar spectral property for the overtone of D mode, so-called $2D$ or G' mode and other dispersive modes.^{7,13} The excitation-energy dispersion of the D mode has been successfully resolved by the double resonance process.^{20–22} Based on the double resonance Raman theory, Grüneis *et al.* recently obtained the phonon dispersion relations of two-dimensional graphite by fitting the experimental frequencies of dispersive Raman modes in graphite materials.²³ The gen-

eralized double resonance process also successfully interpreted the observed two new dispersive phonon modes of the resonantly-enhanced TA and LA phonons⁷ and other dispersive modes in carbon materials.²⁰ However, the observed frequency difference between Stokes and anti-Stokes components (FDSA) of the D mode and other dispersive modes in graphite materials is still an open question to be resolved.⁷

Phonon energy dispersion relation is a fundamental physical property of a solid especially for determining the mechanical, thermal and other condensed-matter phenomena.^{9,23} Because of a slight difference of the electronic structure and phonon dispersion curves of different graphite materials resulting from the different local properties, the dispersive mode may have different values in different graphite materials. For examples, by 1.96-eV excitation, the frequencies of the D mode in graphite whisker⁷ and single-walled carbon nanotubes¹¹ are 1333 and 1323 cm^{-1} , respectively. On the other hand, for a fixed sample, because of the limit of experimental conditions, it is very inconvenient to measure the frequency of the dispersive Raman modes by excitations in a wide energy range, and then to precisely determine the phonon dispersion curves of graphite.

In this paper, we study the Stokes and anti-Stokes scattering spectra of MWNT sample using four different laser excitations. The results show that the frequency of an anti-Stokes Raman mode excited by the excitation energy ε_L is equal to that of the corresponding Stokes Raman modes excited by a higher excitation energy of $\varepsilon_L + \hbar\omega_S$, where $\hbar\omega_S$

is the one-phonon energy of the Stokes mode. We interpret this result by the intravalley and intervalley double resonance process of Stokes and anti-Stokes Raman scattering based on the generalized double resonance model. Because of the peculiar properties of the anti-Stokes Raman scattering, by only a few laser excitations, we here probe the phonon dispersion relations of graphite in a wide range of phonon wave vector from the double resonance processes of Stokes and anti-Stokes Raman scatterings.

II. EXPERIMENT

MWNT samples were as-grown product prepared by the arc method at Clemson.²⁴ The Raman spectra of MWNT's were recorded by two micro-Raman systems (Dilor Super Labram and Dilor Infinity) with a typical resolution of 1–2 cm^{-1} in a back-scattering geometry at room temperature. The two systems consist of holographic notch filters for Rayleigh rejection and a microscope with 100 \times objective lens, allowing a spatial resolution of $\sim 1.0 \mu\text{m}$. The laser excitation wavelengths are 488.0 nm (2.54 eV) and 514.5 nm (2.41 eV) of an Ar⁺ laser, 632.8 nm (1.96 eV) of a He-Ne laser, and 785nm (1.58 eV) of an Al_xGa_{1-x}As diode. Typically, a low laser power of 0.1 mW arrived at the sample was used to avoid sample heating.²⁵ For different laser excitations, different laser powers (from 2 to 10 mW) were used to measure the anti-Stokes Raman signal in MWNT's. All Raman lines at Stokes and anti-Stokes sides are carefully calibrated by Ne lamp under the same experiment conditions, and peak parameters are obtained by least-squares fitting Lorentzian line shapes to the measured spectra. The anti-Stokes Raman spectra have been multiplied by the correction factor $I_s/I_{AS} = (\epsilon_L - E_{\omega_s})^4 / (\epsilon_L + E_{\omega_s})^4 \times \exp(\hbar\omega_s/k_B T)$ and are drawn together with the Stokes spectra with the same x-scale for convenience in comparing them with each other.^{7,25}

III. RESULTS AND DISCUSSIONS

A. Assignment of the observed Raman modes in MWNT's

Figure 1 shows the Stokes and anti-Stokes Raman spectra of MWNTs in the first- and second-order spectral range obtained with the excitation energies of 1.58 and 1.96 eV, respectively. The first-order Stokes and anti-Stokes Raman spectra of C⁺ implanted highly oriented pyrolytic graphite (C⁺ implanted HOPG, CHOPG) excited by $\epsilon_L = 1.58 \text{ eV}$ are also plotted in Fig. 1.

In Fig. 1(a), in addition to the well-known *D*, *G*, *2D*, *D* + *G*, and *2D'* modes located at 1306, 1572, 2606, 2889, and 3205 cm^{-1} , there are two additional high-frequency modes at 1775 and 1871 cm^{-1} and two additional low-frequency modes located at 181 and 280 cm^{-1} . Two dispersive TA and LA low-frequency phonon modes at about 250–500 cm^{-1} have been observed in graphite whisker.⁷ After considering their phonon energies at Γ are equal to zero, we can get their frequency dependences on the excitation energy as the following equations from the Raman data of the resonantly enhanced TA and LA phonon modes in graphite whisker $\omega_{\text{TA}} = 118(\text{cm}^{-1}/\text{eV}) \epsilon_L$, and $\omega_{\text{LA}} = 189(\text{cm}^{-1}/\text{eV}) \epsilon_L$. According to the above equations, the excitation energy of ϵ_L

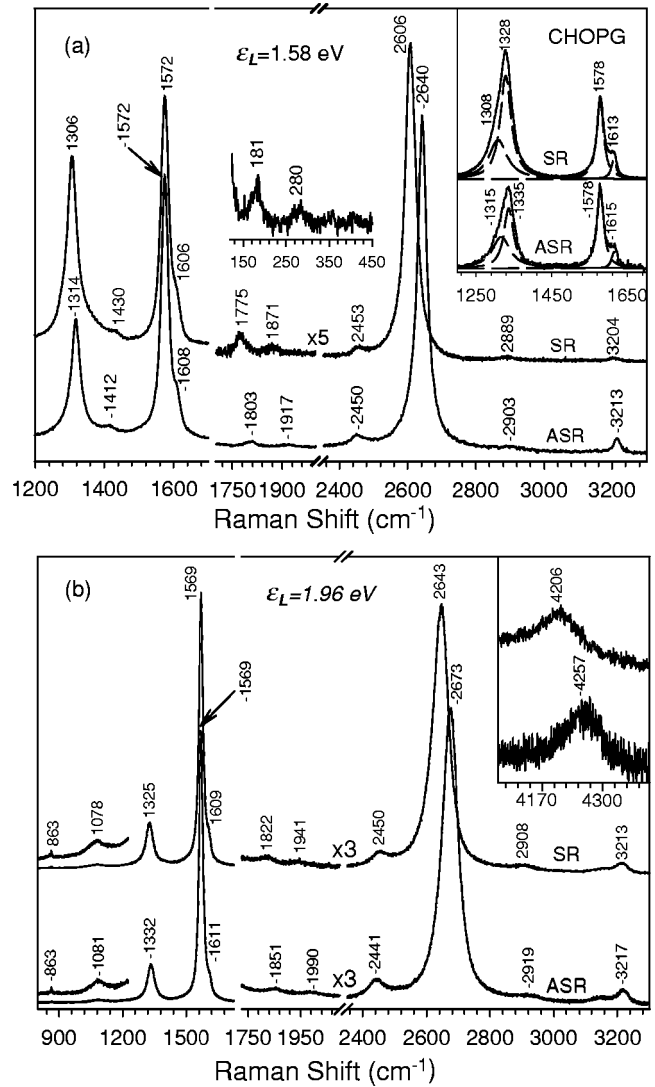


FIG. 1. Stokes (SR) and anti-Stokes Raman (ASR) spectra of MWNT's excited with 1.58 eV (a) and 1.96 eV (b) excitations in the first- and second-order spectral range. The left inset to (a) gives the Stokes Raman spectra of MWNT's in the range of 130–450 cm^{-1} , and its right inset shows the Raman spectra of C⁺ implanted HOPG where the dashed lines give the peaks used to fit the spectra. The inset to (b) shows the SR and ASR spectra of 2*D* + *G* mode.

$= 1.58 \text{ eV}$ can resonantly probe the TA and LA phonon modes at 186 and 298 cm^{-1} , which are close to that of two observed low-frequency modes. Therefore, according to the assignment in graphite whisker,⁷ we assign the two low-frequency modes as *L*₁ and *L*₂ modes. According to the frequency match, the two high-frequency modes at 1775 and 1781 cm^{-1} can be designated as *L*₁ + *G* and *L*₂ + *G* modes. However, after considering the wave vector selection rule of the second-order dispersive modes in graphite materials,²⁶ it is more reasonable to assign the two modes at 1775 and 1871 cm^{-1} as *L*₁ + *D'* and *L*₂ + *D'* modes, respectively.

A band at 863 cm^{-1} appears in the Raman spectra of MWNT's in Fig. 1(b). We observed a mode at 861 cm^{-1} in CHOPG with 1.96 eV laser excitation too.⁷ It is plausible to assign the 861- cm^{-1} mode in CHOPG as the resonantly en-

hanced phonon mode of the out-of-plane TO phonon branches near the Γ point because its frequency is 6 cm^{-1} smaller than that of Γ -center A_{2u} mode.²⁰ The frequency of 863-cm^{-1} mode is close to that of the 861-cm^{-1} mode in ion-implanted HOPG, however, it must be pointed out that the frequencies of all the Raman modes of MWNT's in Fig. 1 redshift due to the laser-heating effect that makes one measure the anti-Stokes Raman signals easily.¹³ When using a weaker laser power, the 863-cm^{-1} band blueshifts to 867 cm^{-1} , which is almost equal to the frequency of infrared-active A_{2u} mode.^{1,27} The close agreement and the sharpness (full width at half maximum intensity, 3.5 cm^{-1}) of the 867-cm^{-1} feature in MWNT imply that it can be related to the vibrational mode corresponding to the out-of-plane A_{2u} at Γ point, which becomes Raman active due to a point symmetry change because of the tubular structure in nanotubes and the presence of structural defects and disorders in MWNT's.

Figure 1 also shows a mode at 1076 cm^{-1} . Because the diameter of MWNT is so large that the size-dependent zone-folding effect is not important for the frequency of Raman modes in MWNT, the spectral characteristics of graphite whisker, HOPG and MWNT are similar to each other.^{3,7} Thus, the bands at 1076 and $\sim 2453\text{ cm}^{-1}$ are designated as D'' and $D''+D'$ modes based on the assignment in graphite whisker.⁷ For the Raman spectra in graphite whisker,⁷ only a single band at 1130 cm^{-1} is observed by the 1.96-eV excitation at the room temperature. However, with increasing the sample temperature, the intensity of the 1130-cm^{-1} mode decreases and a new mode is revealed at 1079 cm^{-1} (see Fig. 10 of Ref. 7), which is very close to the 1076-cm^{-1} observed in MWNT's. According to the recent theoretical calculation on the dispersion curves of graphite based on the double resonance theory,²³ we assign the lower-energy part of the D'' mode in graphite whisker and the 1076 cm^{-1} mode in MWNT's as the phonon modes near the K point to the in-plane TA phonon branches, and the high-energy part of the D'' mode in graphite whisker as the resonantly selected phonon modes near $3K/4$ point to the LA phonon branches.

B. Frequency discrepancy between Stokes and anti-Stokes Raman modes in MWNT's

We now analyze the Stokes and anti-Stokes Raman spectra of MWNT. Similar to the FDSA results in graphite whisker,⁷ HOPG and CHOPG,¹³ the frequencies of the anti-Stokes D , $2D$, $D+G$ modes are larger than those of the corresponding Stokes modes, while the Stokes and anti-Stokes lines of the G mode have the same frequencies as the common theoretical prediction. At the same time, the $2D'$ mode and two new observed L_1+D' and L_2+D' modes also show different frequencies between Stokes and anti-Stokes sides whose values are, respectively, 6 , 29 and 49 cm^{-1} by 1.96-eV excitation. The nonzero FDSA value of the $2D'$ mode indicates that the D' mode is a little dispersive in MWNT, which results from the double resonance Raman effect in graphite materials.^{20,23}

The Stokes and anti-Stokes Raman spectra of MWNTs excited by 2.54-eV excitations are also measured and shown in Fig. 2. In contrast to the Raman spectra of HOPG,

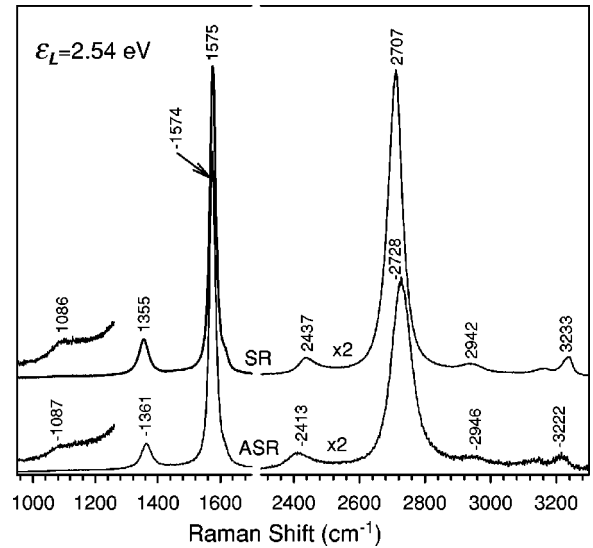


FIG. 2. First- and second-order Stokes (SR) and anti-Stokes Raman (ASR) spectra of MWNT's obtained with 2.54-eV excitation.

CHOPG, and graphite whisker,^{7,13} the Stokes and anti-Stokes Raman spectra in MWNT's exhibit the following different features. First, some FDSA values of dispersive modes in MWNT's are much different from those in HOPG and CHOPG. For examples, for the 1.96-eV excitation, the FDSA value of the $D''+D$ mode is 20 cm^{-1} in CHOPG, while that in MWNT's is 9 cm^{-1} . The FDSA value of the $2D$ mode is 33 cm^{-1} in graphite whisker, which is 3 cm^{-1} higher than that in MWNT's. Second, the FDSA values in MWNT's strongly depend on the excitation energy ϵ_L , while the FDSA values in HOPG and CHOPG are almost insensitive to the excitation energy when the excitation is in the range between 2.54 and 1.96 eV . The Stokes and anti-Stokes Raman spectra of CHOPG excited by 1.58-eV excitation are shown in Fig. 1. The FDSA values of the double peaks of the D mode in CHOPG are 7 cm^{-1} , which is equal to those excited by 1.96- , 2.41- , and 2.54-eV excitations. However, the FDSA value of the $D(2D)$ mode in MWNT's changes from 7.7 (33.5) cm^{-1} to 6.3 (21.4) cm^{-1} when the excitation energy increases from 1.58 eV to 2.54 eV . We summarize all the data about the FDSA values in MWNT's excited with difference sources in Table I. To get the frequencies of Raman modes at room temperature, the Raman spectra of MWNT's are measured using very low laser density and the frequencies of all Raman modes by four excitations are summarized in Table I.

The experimental data have shown that the FDSA value of a dispersive mode in graphite whisker is determined by its phonon energy and its frequency dispersion on the excitation energy⁷

$$\Delta\omega(\epsilon_L)|_{\text{exp}} = \hbar\omega_s \frac{\partial\omega_s}{\partial\epsilon_L}. \quad (1)$$

If the peak frequency of a Raman mode is linear to the excitation energy, from Eq. (1), one gets that the FDSA value of the Raman mode should be independent of the excitation

TABLE I. Frequency discrepancy ($\Delta\omega$) between the Stokes (S) and anti-Stokes (AS) components of certain Raman modes in MWNTs excited by 1.58-, 1.96-, 2.41-, and 2.54-eV excitations where $\Delta\omega = |\omega_{AS}| - |\omega_S|$. The blank cells indicate that those modes are silent, or their positions are not easy to be determined due to weak intensity and low signal-to-noise ratio. $\partial\omega_S/\partial\varepsilon_L$ is the laser-energy dispersion of the Stokes mode, and it is an average value for some modes (e.g., D' , $D+D''$, $2D'$, etc.) because the frequencies of those modes are nonlinear to the excitation energy.

Assign.	D''	D	G	D'	L_1+D'	L_2+D'	$D''+D$	$2D$	$D+G$	$2D'$	$2D+G$
$\partial\omega_S/\partial\varepsilon_L(\text{cm}^{-1}/\text{eV})$	3	45	0	9	130	188	-18	104	48	20	102
$\omega_{S,1.58\text{ eV}}(\text{cm}^{-1})$		1314	1582	1615	1785	1882	2466	2619	2907	3227	
$\Delta\omega_{1.58\text{ eV}}(\text{cm}^{-1})$		7.7	0	2	28	46	-3	33.5	14	9	
$\omega_{S,1.96\text{ eV}}(\text{cm}^{-1})$	1087	1335	1581	1621	1834	1956	2467	2662	2931	3237	4245
$\Delta\omega_{1.96\text{ eV}}(\text{cm}^{-1})$	3	7.2	0	2	29	49	-9	30.0	11	6	51
$\omega_{S,2.41\text{ eV}}(\text{cm}^{-1})$	1093	1353	1582	1623		2038	2453	2708	2948	3245	4291
$\Delta\omega_{2.41\text{ eV}}(\text{cm}^{-1})$	-3	5.7	-1				-18	24.1		-3	40
$\omega_{S,2.54\text{ eV}}(\text{cm}^{-1})$	1089	1358	1583	1624	1910	2063	2451	2718	2953	3247	4303
$\Delta\omega_{2.54\text{ eV}}(\text{cm}^{-1})$	1	6.3	-1				-24	21.4	4	-11	

energy. This phenomenon has been observed in the Stokes and anti-Stokes Raman spectra of HOPG and CHOPG within the laser-energy range of 1.58–2.55 eV.¹³ The laser-energy dependent FDSA values of Raman modes in MWNT imply that the value of $\partial\omega_S/\partial\varepsilon_L$ in MWNT is nonlinear to the excitation energy ε_L . Figure 3 shows the excitation-energy dependence on the Stokes and anti-Stokes Raman frequencies of the D , D' , $2D$, and $2D'$ modes in MWNT's, in which the anti-Stokes frequencies of the four modes at room

temperature are calculated by the FDSA values adding the corresponding Stokes frequencies measured with very low laser density. It is clear that, for MWNT samples, the frequency dependence of Stokes and anti-Stokes components of the D , D' , $2D$, and $2D'$ modes is nonlinear to the excitation energy in the observed energy range of 1.55–2.55 eV. It results in that the FDSA value of the $2D$ mode in MWNT's even changes from 30 cm^{-1} by 1.96-eV excitation to 21.4 cm^{-1} by 2.54-eV excitation while that in HOPG is almost a constant of 27 cm^{-1} within the excitation range of 1.96–2.54 eV.¹³ The FDSA value of the $2D'$ mode in MWNT's even changes from a positive value (9 cm^{-1} , 1.58 eV) to a negative value (-11 cm^{-1} , 2.54 eV). The different FDSA values of Raman modes in HOPG and MWNT indicate the slight difference between the electronic structure and phonon dispersion relation between HOPG and MWNT because of the coupling between the A and B graphene layers that are stacked in the highly ordered $\cdots ABAB \cdots$ structure.

C. Double resonance mechanism for the Stokes and anti-Stokes spectra of first-order Raman modes and their overtones in graphite

To quantitatively interpret the observed FDSA values for the dispersive Raman modes in HOPG, graphite whisker and MWNT, we must carefully discuss the difference of the Stokes and anti-Stokes resonance Raman processes.²⁸ In addition to the D mode and its overtones, there also exist other dispersive modes, such as the D' , D'' , L_1 , and L_2 modes and their overtones. The D and D'' modes are explained by an intervalley double resonance mechanism, which occurs around two inequivalent K points at neighboring corners of the first Brillouin zone of graphite, and the D' , L_1 , and L_2 modes are explained by an intravalley double resonance mechanism, which occurs around the K point in the two-dimensional Brillouin zone of graphite.^{20,23} Because the intravalley and an intervalley double resonance processes are similar to each other, here we only focus our attention on the intravalley double resonance processes to explain the Stokes and anti-Stokes spectra of the D' , L_1 , and L_2 modes and their overtones.

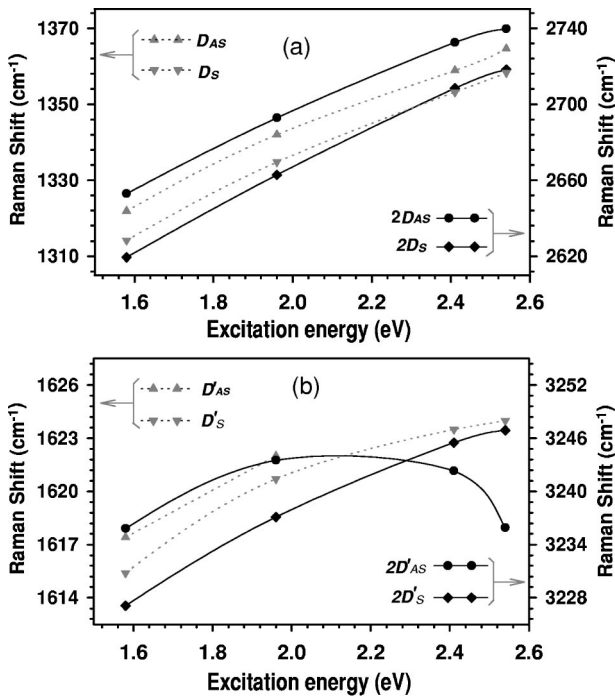


FIG. 3. Stokes (S) (gray down-triangles and solid diamonds) and anti-Stokes (AS) (gray up-triangles and solid circles) Raman frequencies (a) of the D and $2D$ modes, and (b) of the D' and $2D'$ modes in MWNT's as the function of the excitation energy ε_L . The gray and solid lines are a guide to the eye for the frequency dependence of first-order Raman modes and their overtones on the excitation energy, respectively.

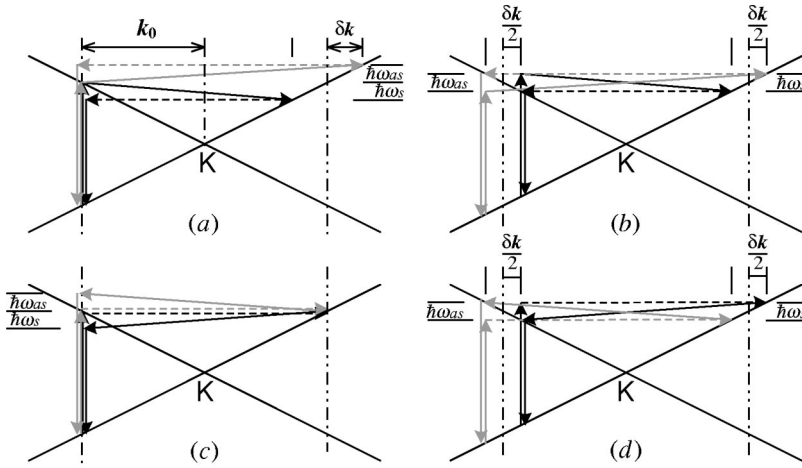


FIG. 4. Schematic diagram of four intravalley double resonance Stokes (black lines) and anti-Stokes (gray lines) processes. The dashed lines mean an elastic scattering process.

For the double resonance process in graphite, an electron with momentum k [and electron energy $E^i(k)$] is first excited by the incident laser photon in an electron-hole creation process. The electron is then scattered by emitting or absorbing a phonon with momentum q to the state with momentum $k + q$ [and energy $E(k + q)$], then scattered again, back to the state with momentum k [and electron energy $E^f(k)$] to recombine with a hole. In general, there exist four possible double-resonance scattering mechanisms for the Stokes and anti-Stokes scattering processes.²⁰ Those four processes can be classified by either an incident or scattered resonance Raman event, and by the fact that either an elastic or inelastic event occurs first. Figure 4 shows the four possible intravalley double resonance processes of Stokes (solid lines) and anti-Stokes (gray lines) Raman scatterings, in which (a) denotes incident resonance, inelastic first, (b) scattered resonance, inelastic first, (c) incident resonance, elastic first, and (d) scattered resonance, elastic first. The difference between Stokes and anti-Stokes Raman scatterings is that the inelastic scattering of the double resonance process occurs with a phonon emission or a phonon absorption process. For the first-order Raman modes, the above four processes are possible to contribute to the double resonance scattering of Stokes and anti-Stokes spectra.

The resonantly selected phonon vectors can be calculated from the energy-momentum conservation condition of the double resonance process. For the double resonance process of a first-order Raman mode, $E(k + q)$ is always one of the resonant states. For cases of the incident and scattered resonances $E^i(k)$ ($=\epsilon_L$) and $E^f(k)$ ($=\epsilon_L \pm \hbar\omega_{ph}$) are, respectively, the second resonant states, in which ϵ_L is the photon energy of an excitation. Because electrons have a linear energy dispersion relation near the K point of graphite, to a first-order approximation, the equienergy contours of $E(k)$ can be treated as circles with a vector of k from the K point,^{20,23,28} where $E(k) = Ak$ in which $A = \sqrt{3}\gamma_0 a/2$, a is graphite lattice constant and γ_0 ($=2.90$ eV) the tight-binding overlap integral parameter. The equienergy contour of a phonon energy ($\hbar\omega_{ph}$) thus corresponds to a vector of δk ($=\hbar\omega_{ph}/A$). For the Stokes case in Fig. 4(a), ϵ_L is equal to the energy separation between the π and π^* bands with a vector k_0 [$=(\epsilon_L/2)/A$] from the K point, the other resonant energy of Stokes process corresponds to a circle near the K

point with a radius of $k_0 - \delta k$. The phonon vector q can be determined by the vector transition between two points along the circles with radii of k_0 and $k_0 - \delta k$ around K , in which the distribution of possible q values has a one-dimensional Van Hove singularity at $q = \delta k$ and $q = 2k_0 - \delta k$. The phonons associated with the second singularity give a significant contribution to the intravalley double resonance process of the observed Raman modes, such as the D' , L_1 , and L_2 modes. We can also apply the same analysis to the other double resonance processes of the first-order Raman mode. There are other three possible singularities at $q = 2k_0 - \delta k$, $q = 2k_0$ and $q = 2k_0$ for the Stokes cases in Figs. 4(b), 4(c), and 4(d), respectively, which contribute to the double resonance process. There also exist four possible singularities at $q = 2k_0 + \delta k$, $q = 2k_0 + \delta k$, $q = 2k_0$ and $q = 2k_0$ that contribute to the double resonance Raman scattering of the anti-Stokes processes in Figs. 4(a), 4(b), 4(c), and 4(d), respectively.

For the overtones such as the $2L_1$ and $2D'$ modes, the double resonance process will involve two phonons, instead of one phonon and one defect. Thus, there only exist two possible resonant processes for an overtone of the first-order mode, which can be classified by either an incident or scattered resonance Raman event. Applying the above analysis to the Stokes and anti-Stokes overtones, only phonons with $q = 2k_0 - \delta k$ and $q = 2k_0 + \delta k$ contribute to the overtones of Stokes and anti-Stokes Raman peaks.

The above analysis can also be applied to the intervalley double resonance Raman process,²⁸ which is responsible for the frequency dispersion of the D'' mode, the D mode and its overtone $2D$ mode. In short, if we assume that the frequencies related to the phonon vectors $|2k_0 - \delta k|$, $|2k_0|$, and $|2k_0 + \delta k|$ measured from the K point (intervalley resonance process) or Γ point (intravalley resonance process) are, respectively, ω_- , ω_0 and ω_+ , a first-order Raman mode based on the double resonance Raman mechanism should contain two peaks and its overtone only has one peak, in which the first-order Stokes peak consists of two peaks with frequencies ω_- and ω_0 , its anti-Stokes component contains two peaks with frequencies ω_0 and ω_+ , and the Stokes and anti-Stokes overtones have the frequencies of $2\omega_-$ and $2\omega_+$, respectively.

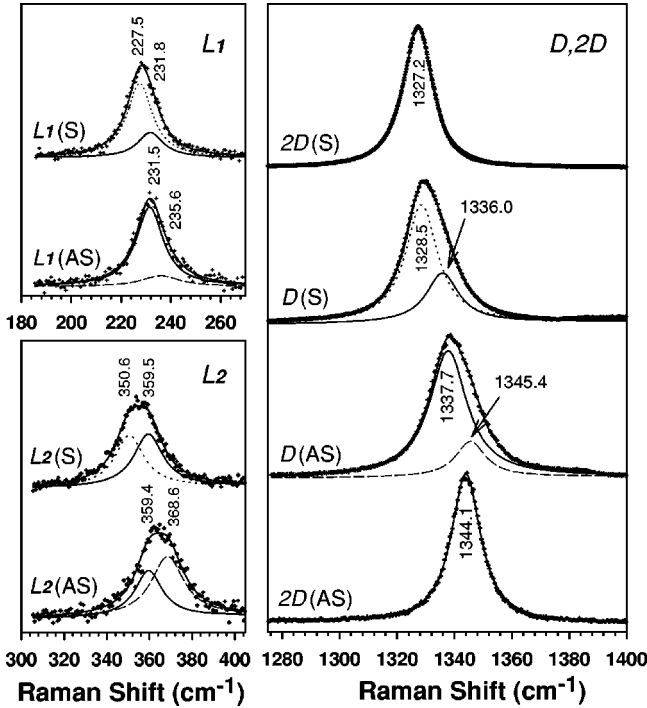


FIG. 5. Stokes (*S*) and anti-Stokes (*AS*) Raman spectra of the L_1 , L_2 , and D modes and the overtone $2D$ mode in graphite whiskers excited by 632.8 nm laser excitation. The frequency of the $2D$ mode has been divided by two to have the same frequency scale as the D mode. The Stokes and anti-Stokes peaks of each first-order mode have been fitted by the peaks ω_- (dotted lines), ω_0 (solid lines), and ω_+ (dashed lines).

Because of the broadened width (up to 50 cm^{-1} for D mode) of certain Raman peaks in graphite materials induced by finite-crystal-size effects and defects, two peaks that only have a frequency separation of several wavenumber almost cannot be clearly resolved from a broad first-order Raman mode. To check the two-peak behavior in the first-order Raman modes of graphite materials, we discuss the Stokes and anti-Stokes spectra of the L_1 , L_2 , and D modes of graphite whisker because Raman peaks in graphite whisker have much smaller widths than other materials.⁷ Figure 5 clearly shows that the Stokes and anti-Stokes L_2 modes do not exhibit a Lorentzian line shape and the Stokes and anti-Stokes components of the L_1 and D modes reveal asymmetric profiles. We use two Lorentzian peaks at ω_- and ω_0 to fit the D mode in the Stokes side, and two Lorentzian peaks at ω_0 and ω_+ to fit the D mode in the anti-Stokes side. Moreover, we use two single Lorentzian peaks at $2\omega_-$ and $2\omega_+$ to separately fit the $2D$ mode in the Stokes and anti-Stokes spectrum. In the fitting process, three Lorentzians at ω_- , ω_0 and ω_+ keep almost the same peak widths, but their intensities are adjustable to get a good fitting to the asymmetric profile of the D mode at Stokes and anti-Stokes sides. We also apply the similar fitting to the Stokes and anti-Stokes spectra of the L_1 and L_2 modes. Seen from Fig. 5, two Lorentzian peaks can give a good fit to the Stokes and anti-Stokes first-order modes. Obviously, the Stokes and anti-Stokes L_2 peaks can be decomposed into two peaks with almost the same

intensities and locate at $(\omega_- + \omega_0)/2$ and $(\omega_0 + \omega_+)/2$. However, the low-energy peaks of the L_1 and D modes are much stronger than their high-energy peaks. Thus, for the L_1 and D modes, their Stokes peaks appear at ω_- and their anti-Stokes peaks at ω_0 , but the Stokes and anti-Stokes $2D$ modes still locate at $2\omega_-$ and $2\omega_+$, respectively. This results in that the Stokes $2D$ mode of graphite whisker is almost centered at two times the Stokes D -mode frequency, but the anti-Stokes $2D$ mode is about $2(\omega_+ - \omega_0)$ higher than the two times frequency of the anti-Stokes D mode.

For the intervalley and intravalley double resonance process, Raman results in graphite whisker show that the Stokes and anti-Stokes lines of the L_2 center at the frequencies relative to the wave vectors of $2k_0 - \delta k/2$ and $2k_0 + \delta k/2$ [$=2(k_0 + \delta k/2) - \delta k/2$], and those of the L_1 and D modes appear at the frequencies relative to the wave vectors of $2k_0 - \delta k$ and $2k_0$ [$=2(k_0 + \delta k/2) - \delta k$], respectively, where $2k_0$ and $2(k_0 + \delta k/2)$ separately correspond to the excitation energies of ε_L and $\varepsilon_L + \hbar\omega_S$. From the above expressions in two brackets, we can get an important relation between the frequencies of Stokes and anti-Stokes peaks

$$\omega_{AS}(\varepsilon_L) = \omega_S(\varepsilon_L + \hbar\omega_S). \quad (2)$$

For a dispersive mode (e.g., the L_2 mode) that is composed by two peaks with almost the same intensity, the ω_{AS} and ω_S in Eq. (2) correspond to the average frequency value of the two peaks of the dispersive mode. Eq. (2) indicates that the frequency ω_{AS} of an anti-Stokes peak excited by an excitation of ε_L is equal to that of the corresponding Stokes peak excited by a laser excitation of $\varepsilon_L + \hbar\omega_S$. For an overtone, its Stokes and anti-Stokes peaks have the frequencies of $2\omega_-$ and $2\omega_+$, and thus we have the following expression to derive the frequency of an anti-Stokes overtone from that of the corresponding Stokes overtone:

$$2\omega_{AS}(\varepsilon_L) = 2\omega_S(\varepsilon_L + 2\hbar\omega_S). \quad (3)$$

Eq. (3) can be deduced from Eq. (2) just replacing the frequency (ω_{ph}) of the first-order peak with that ($2\omega_{ph}$) of its overtone.

Beside the first-order Raman modes and their overtones, we find that Eq. (2) can also be applied to the other combination modes ($L_1 + L_2$, $L_1 + D'$, $L_2 + D'$, $D + G$, $2D + G$, etc.). For example, the FDSA value of the $2D + G$ mode is 51 cm^{-1} by 1.96-eV excitation, which is very close to the Stokes frequency difference (57 cm^{-1}) of the $2D + G$ mode by two different excitations of 1.96 eV and 2.54 eV ($=1.96 \text{ eV} + \hbar\omega_{2D+G} + 0.04 \text{ eV}$) where an additional energy of 0.04 eV contributes to the additional Stokes frequency difference of 6 cm^{-1} . If the frequency of a dispersive mode has a linear relation to the excitation energy, the FDSA value of the dispersion mode is simply related with the phonon energy and its excitation-energy dispersive behavior

$$\begin{aligned} \Delta\omega(\varepsilon_L) &= \omega_{AS}(\varepsilon_L) - \omega_S(\varepsilon_L) \\ &= \omega_S(\varepsilon_L + \hbar\omega_S) - \omega_S(\varepsilon_L) \\ &= \hbar\omega_S \frac{\partial\omega_S}{\partial\varepsilon_L}. \end{aligned} \quad (4)$$

This equation has been confirmed by the experimental data of the Stokes and anti-Stokes Raman spectra of graphite whisker.⁷

Usually, Stokes Raman spectra can only provide the information of first-order dispersive modes, because the frequency of a higher-order Raman mode is just the sum of the frequencies of its fundamental modes. Equation (2) suggests that the frequency ω_S of a first-order or higher-order Stokes mode by excitation $\varepsilon_L + \hbar\omega_S$ can be detected by the frequency ω_{AS} of the corresponding anti-Stokes mode by excitation ε_L . For example, the anti-Stokes frequency of the $2D'$ mode by 2.54-eV excitation is 3235 cm^{-1} , then we can get the Stokes frequency of the $2D'$ mode by 2.94-eV ($2.54 \text{ eV} + \hbar\omega_{2D'}$) excitation are 3235 cm^{-1} . Therefore, the anti-Stokes modes provide more information on the excitation-energy dispersion properties of dispersive Raman modes.

D. Phonon dispersion relation of graphite determined from double resonance Stokes and anti-Stokes Raman processes

The dispersive properties of anti-Stokes Raman modes allow us to probe the phonon dispersion relations of graphite materials by the double resonance anti-Stokes Raman process. From the frequency (ω_{AS}) of an anti-Stokes mode excited by an excitation of ε_L , we can obtain the frequency of the corresponding Stokes mode excited by $\varepsilon_L + \hbar\omega_{AS}$. Together with the frequencies of Stokes modes, there are several pairs of the Stokes frequency and its excitation energy. If neglecting the trigonal warping effect,²⁹ a Stokes first-order mode locates at the frequency relative to the wave vector of $2k_0 - \delta k/2$ while its overtone is contributed from the phonon with the wave vector of $2k_0 - \delta k$,³⁰ in which wave vectors $2k_0$ and δk are determined by the excitation and phonon energies, respectively. In this way, the frequencies and wave vectors of the first-order peak and its overtone can be determined. By using a simple tight-binding electronic energy calculation with tight-binding overlap energy parameter $\gamma_0 = 2.90 \text{ eV}$,³¹ we can obtain the wave vector k of the electronic state that resonant with an excitation energy, and then get the phonon wave vector q of the observed phonon mode. We calculate the phonon wave vectors contributed to the anti-Stokes and Stokes components of L_1 , L_2 , D , D' , $2D$, $2D'$, and $2D+G$ modes excited by four excitation energies, and plot them in Fig. 6 together with the recent calculated phonon dispersion relations of graphite. To get the phonon dispersion relation of two acoustic modes, we also add some data of the L_1 and L_2 modes in graphite whisker.⁷

The frequency data of the dispersive D mode shown in Fig. 6 are in good agreement with the recent fitted phonon dispersion relations.²³ The peak frequencies of the D' , L_1 , and L_2 modes are slightly larger than that of the theoretical results, and the highest frequency of the experimentally observed LO phonons is located at 1624 cm^{-1} near the $K/5$ point. Using a polynomial fit to the experimental data of the observed dispersive modes, the frequency of the D and D' modes are almost cubic to the wave vector q within the detected wave vector regions, and their relations are, respec-

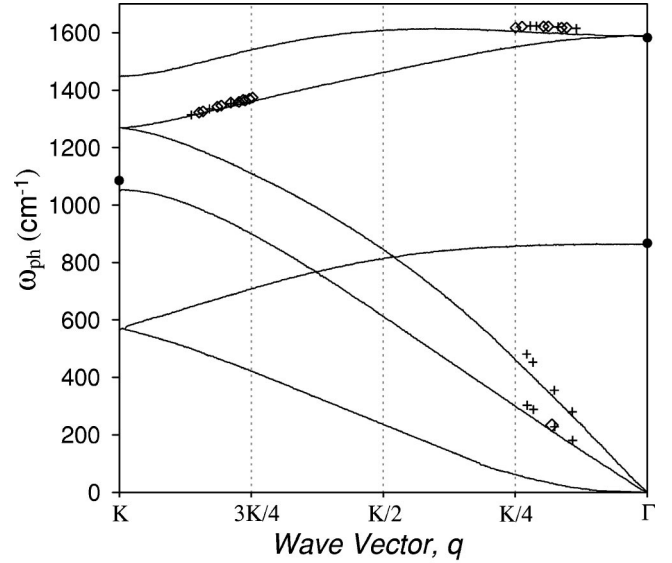


FIG. 6. Experimental data of the phonon dispersion relations of graphite along Γ - K axis determined by the observed frequencies of the Stokes modes (crosses, L_1 , L_2 , D , and D'), anti-Stokes modes (diamonds, D , D' , $2D$, $2D'$, and $2D+G$) and zone-center or edge modes (solid circles, A_{2u} , D'' , and G) in MWNT's. Some experimental data of the L_1 , L_2 , and $2L_1$ modes are obtained from the Stokes and anti-Stokes Raman spectra of graphite whiskers.

tively, $\omega_D(q) = -2355 + 14283q - 17707q^2 + 7052q^3$ ($3/4 < q < 7/8$) and $\omega_{D'}(q) = 1582 + 168q + 1242q^2 - 5316q^3$ ($0 < q < 1/4$), where q is in unit of q_K . The fitting results clearly show that the nonlinear behavior of the phonon dispersion relations of graphite within the detected wavevector regions. Using the dispersive properties of the anti-Stokes modes, only by four excitations, we obtain the experimental data of the phonon dispersion relation in the Brillouin region covered by the excitation energy ε_L from about 1.55 eV to 3.0 eV. Therefore, the anti-Stokes double Raman scattering is very useful to probe the phonon dispersion relations of graphite.

IV. CONCLUSIONS

In summary, the Stokes and anti-Stokes Raman spectra of MWNT's have been studied in this paper by four excitation energies. The observed Raman modes in MWNT's are assigned on the base of the double resonance Raman effect and previous results of graphite whiskers. Many Raman modes in MWNT's have different frequencies between their Stokes and anti-Stokes lines. The values of frequency differences between the Stokes and anti-Stokes lines of Raman modes in MWNT's are strongly dependent on the excitation energy, which is attributed to the nonlinear relations between the frequencies of Stokes and anti-Stokes Raman modes and the excitation energy. For all the dispersive Raman modes, their anti-Stokes peak frequencies excited by ε_L are found to be equal to their corresponding Stokes peak frequencies excited by a laser excitation of $\varepsilon_L + \hbar\omega_S$ where $\hbar\omega_S$ is the phonon energy of each Raman mode. This result is interpreted by the

intravalley and intervalley double resonance process of Stokes and anti-Stokes Raman scattering. Because of the peculiar properties of anti-Stokes Raman scattering, we probe the phonon dispersion relations of graphite from the double resonance process of Stokes and anti-Stokes Raman scatterings. The dispersive Raman data of the D mode are in good agreement with the theoretical results, and the peak frequen-

cies of the L_1 , L_2 , and D' modes are slightly larger than that of the theoretical results.

ACKNOWLEDGMENTS

The authors sincerely thank Professor R. Saito and Dr. Grüneis for providing their unpublished results of two dimensional phonon dispersion relation of graphite.

*Electronic mail: pinghengtan@hotmail.com,
pingheng.tan@wsi.tu-muenchen.de

¹M. S. Dresselhaus and G. Dresselhaus, In *Light Scattering in Solids III*, edited by M. Cardona and G. Guntherodt (Springer, Berlin, 1982).

²P. C. Eklund, J. M. Holden, and J. M. Holden, and R. A. Jishi, *Carbon* **33**, 959 (1995).

³P. H. Tan, S. L. Zhang, K. T. Yue, F. M. Huang, Z. J. Shi, X. H. Zhou, and Z. N. Gu, *J. Raman Spectrosc.* **28**, 369 (1997).

⁴H. Hiura, T. W. Ebbeson, K. Tanigaki, and H. Takahashi, *Chem. Phys. Lett.* **202**, 509 (1993).

⁵A. M. Rao, E. Richter, S. Bandow, B. Chase, P. C. Eklund, K. A. Williams, S. Fang, K. R. Subbaswamy, M. Menon, A. Thess, R. E. Smalley, G. Dresselhaus, and M. S. Dresselhaus, *Science* **275**, 187 (1997).

⁶M. A. Pimenta, E. B. Hanlon, A. Marucci, P. Corio, S. D. M. Brown, S. A. Empedocles, M. G. Bawendi, G. Dresselhaus, and M. S. Dresselhaus, *Braz. J. Phys.* **30**, 423 (2000).

⁷P. H. Tan, C. Y. Hu, J. Dong, W. Shen, and B. Zhang, *Phys. Rev. B* **64**, 214 301 (2001).

⁸S. D. M. Brown, A. Jorio, M. S. Dresselhaus, and G. Dresselhaus, *Phys. Rev. B* **64**, 073 403 (2001).

⁹M. S. Dresselhaus and P. C. Eklund, *Adv. Phys.* **49**, 705 (2000).

¹⁰C. Thomsen, *Phys. Rev. B* **61**, 4542 (2000).

¹¹P. H. Tan, Y. Tang, Y. M. Deng, F. Li, Y. L. Wei, and H. M. Cheng, *Appl. Phys. Lett.* **75**, 1524 (1999).

¹²M. J. Matthews, M. A. Pimenta, G. Dresselhaus, M. S. Dresselhaus, and M. Endo, *Phys. Rev. B* **59**, R6585 (1999).

¹³P. H. Tan, Y. M. Deng, and Q. Zhao, *Phys. Rev. B* **58**, 5435 (1998).

¹⁴I. Pócsik, M. Hundhausen, M. Koós, and L. Ley, *J. Non-Cryst. Solids* **227**, 1083 (1998).

¹⁵Y. Kawashima and G. Katagiri, *Phys. Rev. B* **52**, 10 053 (1995).

¹⁶Y. Wang, D. C. Aolmsmeyer, and R. L. McCreery, *Chem. Mater.* **2**, 557 (1990).

¹⁷A. V. Baranov, A. N. Bekhterev, Y. S. Bobovich, and V. I. Petrov, *Opt. Spektrosk.* **62**, 1036 (1987) [*Opt. Spectrosc.* **62**, 612 (1987)].

¹⁸R. P. Vidano, D. B. Fishbach, L. J. Willis, and T. M. Loehr, *Solid State Commun.* **39**, 341 (1981).

¹⁹S. D. M. Brown, P. Corio, A. Marucci, M. S. Dresselhaus, M. A. Pimenta, and K. Kneipp, *Phys. Rev. B* **61**, R5137 (2000).

²⁰R. Saito, A. Jorio, A. G. Souza Filho, G. Dresselhaus, M. S. Dresselhaus, and M. A. Pimenta, *Phys. Rev. Lett.* **88**, 027 401 (2002).

²¹A. C. Ferrari and J. Robertson, *Phys. Rev. B* **64**, 075 414 (2001).

²²C. Thomsen and S. Reich, *Phys. Rev. Lett.* **85**, 5214 (2000).

²³A. Grüneis, R. Saito, T. Kimura, L. G. Cancado, M. A. Pimenta, A. Jorio, A. G. Souza Filho, G. Dresselhaus, and M. S. Dresselhaus, *Phys. Rev. B* **65**, 155 405 (2002).

²⁴T. W. Ebbesen and P. M. Ajayan, *Nature (London)* **358**, 220 (1992).

²⁵P. H. Tan, Y. Tang, C. Y. Hu, F. Li, Y. L. Wei, and H. M. Cheng, *Phys. Rev. B* **62**, 5186 (2000).

²⁶P. H. Tan, C. Y. Hu, J. Dong, and W. C. Shen (unpublished).

²⁷Y. Kawashima and G. Katagiri, *Phys. Rev. B* **59**, 62 (1999).

²⁸L. G. Cançado, M. A. Pimenta, R. Saito, A. Jorio, L. O. Ladeira, A. Grüneis, A. G. Souza Filho, G. Dresselhaus, and M. S. Dresselhaus, *Phys. Rev. B* **66**, 035415 (2002).

²⁹R. Saito, G. Dresselhaus, and M. S. Dresselhaus, *Phys. Rev. B* **61**, 2981 (2000).

³⁰As shown in Fig. 5, although some first-order Stokes peaks are dominated by the phonons with a wave vector of $2k_0 - \delta k$, the difference between $2k_0 - \delta k$ and $2k_0 - \delta k/2$ is very small and within the experimental accuracy because $\hbar \omega_{ph}/2$ is much smaller than ϵ_L .

³¹R. Saito, G. Dresselhaus, and M. S. Dresselhaus, *Physical Properties of Carbon Nanotubes* (Imperial College Press, London, 1998).